RSC Advances

ROYAL SOCIETY OF CHEMISTRY

www.rsc.org/advances

Journal Name

ARTICLE

Synthesis and characterization of earth-abundant Cu_2MnSnS_4 thin films using a non-toxic solution-based technique

Received 00th January 20xx,
Accepted 00th January 20xx

DOI: 10.1039/x0xx00000x

www.rsc.org/

Leilei Chen[a], Hongmei Deng[b], Jiahua Tao[a], Huiyi Cao[a], Ling Huang[a], Lin Sun[a], Pingxiong Yang[a*] and Junhao Chu[a]

Earth-abundant Cu_2MnSnS_4 (CMTS) thin films were fabricated by a non-toxic spin-coating technique. The precursor solution is based on 2-methoxyethanol solvent of thiourea complex with acetyl-acetone used as additive agent, and the spin-coated films were post-annealed at 570 ºC under a N_2 atmosphere. The influence of annealing time, processed on the precursor films, on the structure, composition, morphology, and optical properties have been studied detailed. We found that longer annealing time during the CMTS growth can improve the phase purity, promote the preferred orientation along (112) direction, and enhance the grain growth in the micrometer range. The film annealed for 10 min gives a pure CMTS phase, whereas other films annealed for lower and/or higher than 10 min (especially 13 min) can be formed secondary phases (i.e., SnS, MnS). The band gap energy is estimated as 1.63~1.18 eV for post-annealed films depending on the heat treatment, compared to 1.69 eV for as-prepared film. An efficiency of 0.49% for the device fabricated here has been achieved with an open-circuit voltage of 308.4 mV, a short-circuit current density of 4.7 mA/cm^2, and a fill factor of 33.9%. It offers a new research direction for the application of CMTS absorber layer in low-cost solar cells.

1. Introduction

Thin film solar cells based on the $Cu(In,Ga)S_2$ (CIGS) have reached a high level of photoelectric conversion efficiency (over 20%).[1] However, gallium and indium used for preparation of the absorber layer are very rare and unceasing used in many industrials, which could lead to a shortage in the supply of these elements and would contributes to the high fabrication costs of CIGS solar cells.[2] Related to the quaternary chalcogenide Cu_2ZnSnS_4 (CZTS), the naturally occurring mineral Cu_2MnSnS_4 (CMTS) has direct band gap energy of 1.0-1.4 eV and a large absorption coefficient of over 10^4 cm^{-1}, properties similar to those of CIGS, which is regarded as one of the potential absorber materials for sustainable and highly efficient solar cells.[3-5] Moreover, compared to CIGS, CMTS consists of abundant and inexpensive Mn and Sn elements that are advantageous for the realization of low-cost solar cells.

Typically, quaternary chalcogenide films such as CIGS and CZTS are deposited by evaporation or sputtering techniques that rely on vacuum environments.[6-8] However, these processes suffer from low throughput and difficulties associated with large scale production. In this consideration, kinds of solution-based approaches have being developed for the synthesis of Cu-based films such as hot-injection,[5, 9] solvothermal,[10] hydrazine-based approach[11, 12] and sol-gel spin-coated.[13-18] Additionally, hot-injection approach and solvothermal method have been employed for the synthesis of CMTS nanoparticles,[5, 10] but there are some limitations. The hot-injection method, whereby precursors are injected into a hot organic medium to instigate the synthesis processes. The solvothermal method also requires a complex reactor autoclave to achieve high pressures for the chemical reactions to proceed. Currently, the record efficiency for CZTSSe devices was obtained by spin-coating a hydrazine-based ink followed by a fast annealing.[12] However, the hydrazine is very unstable and highly toxic which requires extreme caution in handling and storage. Among the solution methods typically used, the spin-coating method is a very simple and low-cost process based on hydrolysis and poly-condensation reactions.[14, 16] With these regard, developing a simple, low-cost and non-toxic spin-coating method is highly desirable for the fabrication of high quality and single phase CMTS material, which is critical to meet the requirements of photovoltaic technologies.

In the present work, we have developed a non-toxic and simple process using a simple solution-based spin-coating method. Conventional aqueous sol-gel processes entail the formation of Metal-O-Metal bonds in the precursor solution or during the annealing step, which can lead to the formation of secondary phases such as binary sulfides ($Cu_{2-x}S$) and oxides (SnO_2), and has a limitation in terms of heat treatment at high temperature.[13, 19] As for the formation of sulfides by sol-gel technique, the process is generally highly active, but toxic hydrogen sulfide gases is used in sulfurizing oxides into sulfides, which makes the prepared thin films not only contain secondary phases, but also show poor surface morphology and weak adhesion to substrates.[15] Here, 2-

[a] Key Laboratory of Polar Materials and Devices, Ministry of Education, Department of Electronic Engineering, East China Normal University, 500 Dongchuan Road, Shanghai 200241, China.
[b] Laboratory for Microstructures, Shanghai University, 99 Shangda Road, Shanghai 200444, China.
* Corresponding author. Tel: +86 21 54345157; fax: +86 21 54345119. E-mail:pxyang@ee.ecnu.edu.cn (P. Yang)

methoxyethanol was used as solvent, and thiourea (TU) was utilized to form Metal-TU complexes. As reported, in aqueous and/or organic solvents, Metal-TU and/or M-TU-M complexes are easily generated.[14] In order to increase the solubility of the precursors and improve the adhesion of the precursor films during the condensation reaction, acetyl-acetone was added as additive agent. Previously, we have reported that the bi-layered structure (a large grain top layer and a small-grain bottom layer) is easily formed in a CZTS-based solar cell processed with a longer deposition time,[20] which can be due to the fact that sulfur is hardly incorporated into the relatively thick CZTS layers. Therefore, rapid thermal processor without sulfurization is utilized to fabricate CMTS films to avoid the formation of bi-layered structure and the influences of post-annealing time on the structural, compositional, morphological and optical properties of the synthesized CMTS thin films were systematically investigated. Also, we have firstly demonstrated the fabrication of CMTS solar cells with a conversion efficiency of 0.49%, based on the spin-coating method.

2. Experimental

2.1 Precursor solution preparation

All chemicals were purchased from Sigma-Aldrich and used as received. In a typical synthesis, $CuCl_2 \cdot 2H_2O$ (7.04 mmol, 99.0%), $SnCl_2 \cdot 2H_2O$ (4.0 mmol, 98.0%), and $Mn(CH_3COO)_2 \cdot 4H_2O$ (4.8 mmol, 99.0%) were used as precursor materials dissolved in 2-methoxyethanol (20 ml, 99.8%) using a magnetic stirrer. Subsequently, thiourea (32 mmol, 99.0%) chosen as sulfur source were added. And then few drops of acetyl-acetone (99.0%) were added as additives. The final solution was stirred for 30 min at 50 ºC to yield a homogeneous, clear and transparent solution. The chemical composition ratios of the raw materials were controlled to have the atomic ratio of Mn/Sn = 1.2 and Cu/(Mn + Sn) = 0.8. This solution was stable for at least several months.

2.2 Film preparation

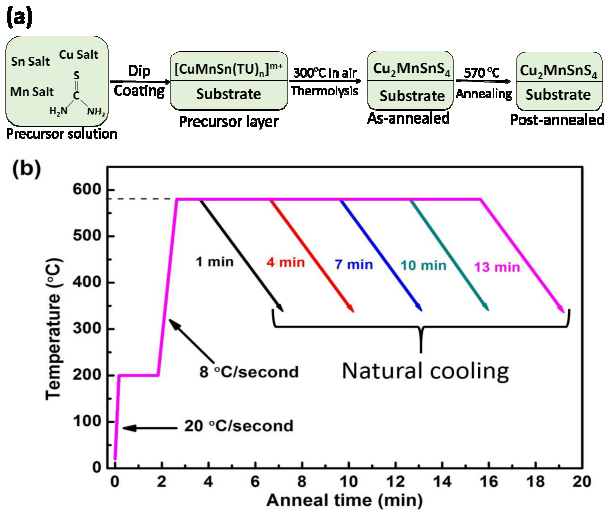

Fig. 1(a) Schematic diagram of CMTS film fabricating sequence, **(b)** post-annealing temperature profile for post-annealing.

CMTS films were deposited via spin-coating the prepared transparent solution on Mo-coated soda-lime glass (SLG) substrates at 3000 rpm for 30 s followed by pre-annealing process at 300 ºC for 3 min. To reach the targeted thickness of the absorber layer, the spin-coating and pre-annealing processes were repeated twelve times. Finally, the post-annealing temperature was fixed at 570 ºC under a N_2 gas flow at a heating rate of 8 ºC/s, and then the samples were cooled naturally to room temperature. The films processing sequence is presented in Fig. 1a. In order to investigate the effect of post-annealing time on the growth of CMTS films, samples 1, 2, 3, 4, 5 were prepared at heat preservation time of 1, 4, 7, 10 and 13 min, the temperature profile was shown in Fig. 1b. The as-prepared and post-annealed CMTS films at 1, 4, 7, 10, and 13 min were designated as CMTS-00, CMTS-01, CMTS-04, CMTS-07, CMTS-10 and CMTS-13, respectively, where numbers represent various annealing time.

2.3 Device fabrication

The completed CMTS solar cell devices with the commonly employed structure of AZO/i-ZnO/CdS/CZTS/Mo/glass were prepared in the present study.[13] The CdS buffer layer with approximately 50-60 nm thickness was grown by chemical bath deposition from an aqueous solution of $CdSO_4$ (1.5 mmol, 99.0%), thiourea (75 mmol, 99.0%) and ammonia (1.8 mmol) at 80 ºC. Then window layers of undoped zinc oxide of about 50 nm thickness and Al-doped ZnO (AZO) of approximately 600 nm thickness were deposited by radio-frequency (RF) magnetron sputtering. Finally, a mechanical scribing step was performed to define the cell area to 0.16 cm^2.

2.4 Characterization

The coating solution was examined via a thermogravimetric analysis (TGA, TA Instrument Q50) under nitrogen atmosphere. The crystalline structures of the as-prepared and post-annealed CMTS films were identified by X-ray diffraction (XRD) using a Bruker D8 Discover diffractometer with Cu Ka radiation (λ=1.54056 Å) from 10° to 70°. The tube voltage and current for the XRD patterns were 40 kV and 40 mA, respectively. Raman scattering experiments were performed with a micro-Raman spectrometer (Jobin-Yvon LabRAM HR 800UV). The morphologies and the chemical composition were characterized by a field emission scanning electronic microscopy (SEM, FEI, S-4700) attached to an energy-dispersive X-ray spectroscope (EDS). The optical properties were determined using transmittance spectra (UV/vis Lambda 2S, Perkin-Elmer). Current-voltage characteristics of the devices were measured under AM 1.5 global spectrum with the irradiance set to 100 mW/cm^2. All measurements were performed at room temperature.

3. Results and discussion

3.1 Synthesis mechanism

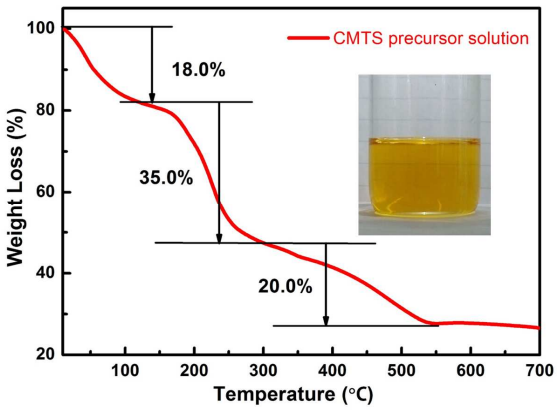

Fig. 2 Thermo-gravimetric analysis of CMTS precursor solution. Inset shows a homogeneous CMTS solution prepared.

The possible mechanism for the synthesis of CMTS precursor complex using the current solution route is as follows. In the solution preparation, firstly, metal salts were added into 2-methoxyethanol, Sn^{2+} ions are oxidized to Sn^{4+} by Cu^{2+}, corresponding to equation (1). Concurrently, when the TU was added into solvent, transparent solution was formed (shown in the inset of Fig. 2) under magnetic stirring for several minutes, which confirms the formation of metal-TU complexes (Cu-Tu, Mn-Tu, and Sn-Tu). Finally, Cu^{+}, Mn^{2+}, Sn^{4+}, and S^{2-} ions in the homogenous solution organize themselves to form the precursor complex. Detailed reaction equations are shown as follows:

$$2Cu^{2+} + Sn^{2+} \rightarrow 2Cu^{+} + Sn^{4+} \quad (1)$$

$$Cu^{+} + nTU \rightarrow [Cu(TU)_n]^{+} \quad (2)$$

$$Sn^{4+} + nTU \rightarrow [Sn(TU)_n]^{4+} \quad (3)$$

$$Mn^{2+} + nTU \rightarrow [Mn(TU)_n]^{2+} \quad (4)$$

$$[Cu(TU)_n]^{+} + [Mn(TU)_n]^{2+} + [Sn(TU)_n]^{4+} \rightarrow [CuMnSn(TU)_n]^{m+} \quad (5)$$

Generally, sol films could be obtained by spin-coating the procedure solution. Subsequently, the sol film was pre-annealed in order to remove organic residues and obtain a dense precursor film. In the meanwhile, the decomposition of the thiourea-metal complexes and the formation of CMTS are involved in this process. In order to gain the decomposition data, the obtained homogenous CMTS precursor solution, as presented in the inset of Fig. 2, was dried at 70 °C for several days and the obtained powder was subjected to TGA. The TGA data in Fig. 2 exhibits a first weight loss stage from room temperature to 140 °C, indicating the thermal evaporation of solvent and water. The second region starts at 140 °C and persists till 300 leading to about 35.0% loss in weight due to thermal decomposition of the Metal-TU complex and excess thiourea. At 300 °C, the formation of CMTS compound is almost completed, and consequently the weight loss rate reduces thereafter. The weight loss still continues at a lower rate to beyond 300 °C which may be due to the decomposition of residual precursor and other volatile organic moieties.[21] It is also noteworthy that the TGA spectrum obtained in this work is similar to those reported for CZTS solutions prepared using the same solvent.[13] Based on above results, we estimate that the pre-annealed temperature required to remove the solvent and other volatile moieties from the precursor and achieve the complete thermal decomposition of the metal-thiourea complexes during the spin coating processes must be above 300 °C.

3.2 Structural studies

3.2.1 XRD characterization

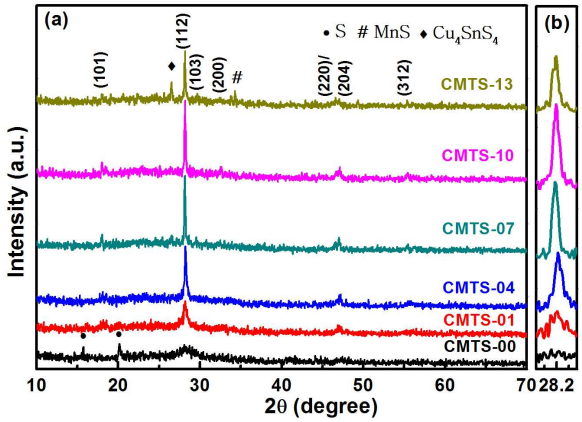

Fig. 3(a) XRD patterns of CMTS films prepared at different annealing time; **(b)** the magnified pattern of (112) peak for 2θ range from 27.7° to 29.7°.

The phase evolution of the CMTS precursor during annealing is presented in Fig. 3a. It can be seen that the as-prepared and post-annealed films with low anneal time (<4 min) show a weak and broad peak at 2θ ≈ 28.21°. Apart from the broad and less intense peak, the S phase (PDF: 65-1101; marked with ●) are detected in CMTS-00 before annealing. For sample CMTS-01, the S phase is not visible anymore and amorphous CMTS phase is formed, which demonstrates that a short annealing time is insufficient for a complete reaction. Upon annealing time up to 4 min, a considerable sharpening in the main diffraction planes occurs, which exhibiting the CMTS phase could become the predominant phase in this condition. Sharp peaks at 2θ ≈ 18.02°, 28.21° and 46.99° can be indexed to the diffraction of the (101), (112), and (220)/(204) planes of stannite CMTS (PDF: 51-0757), respectively. As the annealing time increases to 7 min, the (112) peak shows a dramatical increase, and the other diffraction peaks are well defined without additional impurity peaks, suggesting that as-prepared films could be completely annealed into CMTS at present condition. There is no obvious impurity phase could be observed and the relatively intensity of (112) plane shows a slight increment for CMTS-10, as shown in Fig. 3b, which presents the enlarged 2θ range from 27.7° to 29.7° of the (112) peak of CMTS films. And then the (112) peak intensity decreases as further increasing the annealing time to 13 min. The decrease of (112) peak intensity indicates that too long anneal time lead to the decline of CMTS crystallinity. Additionally, there is the diffraction peaks of secondary phases at 2θ ≈ 26.53° and 34.31° (marked with ♦ and #) can be attributed to Cu_4SnS_4 (PDF: 27-0196) and MnS (PDF: 06-0815) phases, respectively, which indicates that

Table 1 Lattice constants of CMTS films obtained from XRD patterns.

Sample ID	FWHM of (112) peak (degree)	Interplanar spacing of (112) (Å)	Lattice constant *a* (Å)	Lattice constant *c* (Å)	Volume of crystal (Å^3)	Crystallite size D (nm)	Dislocation density δ (lines/m^2)
CMTS-01	0.481	3.152	5.58	10.48	326.31	16.84	35.3×10^{14}
CMTS-04	0.215	3.157	5.55	10.63	327.43	37.68	7.04×10^{14}
CMTS-07	0.172	3.163	5.52	10.80	329.08	47.09	4.02×10^{14}
CMTS-10	0.153	3.165	5.54	10.70	328.40	51.94	3.57×10^{14}
CMTS-13	0.174	3.163	5.54	10.72	329.01	46.82	4.51×10^{14}

further prolonging the annealing time may lead to the decomposition of CMTS films.

The full-width at half-maximum (FWHM) of (112) peak was measured and surmised in Table 1. As presented in Table 1, FWHM decreases from 0.481 to 0.169º as the annealing time increase from 1 min to 10 min, and then slightly increase to 0.174º with further prolonging annealing time to 13 min. It should be noted that structure defects, internal strain and crystallite sizes can be correlated to the width of diffraction peaks. The interplanar spacing of the post-annealed films is increasing with the increase in annealing time, which indicates the internal compressive strain relaxation in CMTS films.[4] Structure defects generally refer to dislocation density and local inhomogeneity *etc.* in polycrystalline to crystal materials. As shown in the following Fig. 5, the composition of all CMTS samples deviates from the stoichiometry of Cu_2MnSnS_4, which implies that there might be exists structure defects. Moreover, the crystallite size (CS) of these samples have been calculated using the Scherer's equation $D = 0.9\lambda/(\beta\cos\theta)$.[13] The CS rises significantly from 16.84 to 48.19 nm with increasing anneal time to 10 min and thereafter it decreases to 46.82 nm due to the degradation of CMTS phase. The dislocation density (δ) values which is defined as the length of dislocation lines per unit volume (lines/m^2) can be obtained from the Williamson Smallman's formula, $\delta = 1/D^2$.[22] The decrease tendency of δ, as presented in Table 1, has demonstrated that the sample annealed for a shorter time has more crystal defects. Moreover, the lattice parameters (i.e. *a* and *c*) were calculated accordance with the Bragg equation.[23] The lattice constants *a* is decreasing with the increase of annealing time, whereas *c* shows an increase tendency. Furthermore, the calculated crystal parameters for the film annealed at 10 min are in good agreement with the reported values.[24]

3.2.2 Raman spectroscopy

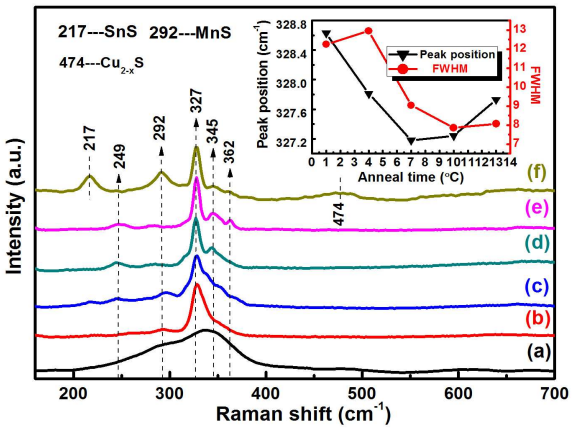

Fig. 4 Room temperature Raman spectra of **(a)** CMTS-00, **(b)** CMTS-01, **(c)** CMTS-04, **(d)** CMTS-7, **(e)** CMTS-10, and **(f)** CMTS-13. Inset is the FWHM and peak position of CMTS films main A_1 mode.

It is observed that 2θ positions of the dominant peak of CMTS and Cu_2SnS_3 (CTS) are very close,[23] which makes it difficult to confirm the CMTS phase from XRD pattern analysis. Therefore, Raman spectroscopy was utilized to obtain further insight into the phase identification. The results of CMTS films as a function of the annealing time are shown in Fig. 4. The as-prepared precursor film exhibits a broad band which encompasses the main modes expected from CMTS or/and CTS. According to the results of TGA, at 300 °C, the formation of CMTS compound is almost completed. Therefore, it might be inferred that the broad band can simply be ascribed to CMTS, but with poor crystallinity. The sample taken at 1 min shows a strong peak positioned at ~328 cm^{-1}, which is attributed to the A_1 mode of CMTS. The A_1 mode in CMTS involves only the anion vibrations and it has been assigned to the most intense lines observed in the experimental Raman spectra.[25] With increasing the annealing time to 4 min, more characteristic peaks of CMTS are resolved. However, the sample CMTS-04 also exhibits a weak peak at 292 cm^{-1} which can be assigned to MnS impurity phase.[26] For the film CMTS-07, a major peak posited at 327 cm^{-1}, along with two weak peaks at 245 cm^{-1} and 345 cm^{-1}, which are consistent with previously reported CMTS values.[23] The film annealed for 10 min appears similar to that annealed 7 min. No evidence of other possible binary phases appears in CMTS-10 Raman spectrum, indicating the pure CMTS phase has been obtained. Moreover, there are no visible peaks which could be attributed to CTS since the characteristic peaks at 260, 298, and 356 cm^{-1} could not be observed.[7, 13, 27] However, the sample CMTS-13 shows additional peaks at 217 and 292 cm^{-1} which can be assigned to SnS and MnS phases, respectively. And a weak peak appears at 474 cm^{-1} indicates the presence of $Cu_{2-x}S$ phase.[28] The SnS phase observed in CMTS-13 is not detected in the XRD pattern, which is possibly due to only a small amount of SnS phase exists.

The effect of annealing time on CMTS films can be better understood by comparing the FWHM values of the dominant A_1 mode, since the sharpness of A_1 mode can reflect the crystalline quality of films.[29] For all those post-annealed films, the FWHM values for main A_1 mode is measured and presented in the inset of Fig. 4. The variation FWHM of the A_1 mode with the change in annealing time is distributed from 12.95 to 7.85 cm^{-1}. Particularly, minimum FWHM, 7.85 cm^{-1}, is for the film annealed for 10 min represent the best crystallinity. Moreover, the main peak position shows a small red-shift with increasing the anneal time and then shift towards high wavenumbers as further increase annealing time to 13 min, which could be related to the presence of impurity phases and/or stress.[30] The present experimental results display that further prolonging annealing time up to 13 min could lead to the decomposition of CMTS phase. Therefore, the annealing time is very important to modulate the secondary phase and fabricate the high quality CMTS films.

3.3 Composition analysis

The elemental composition and compositional ratios of the as-prepared and post-annealed CMTS thin films are presented in Fig. 5. In the annealing time range studied, a general upward trend in the Cu content is observed. The ratio of Cu/(Mn + Sn) exhibits a similar trend as well. The ratio of Mn and Sn seems to be fluctuating which may be due to the evaporation of some components in the form of chalcogenide during annealing at a high temperature (570 °C). It has been reported that, Sn element is easily lost in SnS phase at annealing temperature higher than 400 °C.[28] It still needs further study about chemical kinetics of this material to get stability in cations stoichiometry. Additionally, a dramatical decrease of the S/Metal ratio (from 0.81 to 0.68) and an increase of Cu/(Mn + Sn) ratio (from 0.91 to 2.21) can be observed from Fig. 5b with the post-annealing time ranging from zero to 13 min, which may be arising from the decomposition of CMTS phase and volatilization of S during the long annealing process. A specially post-annealing process may give rise the S-poor state, which may be fine-tuned by increasing the molar concentration of TU incorporated in the solution preparation (Eq. 2, 3, 4). The decomposition of the CMTS annealed for 13min has been confirmed by XRD and Raman measurements.

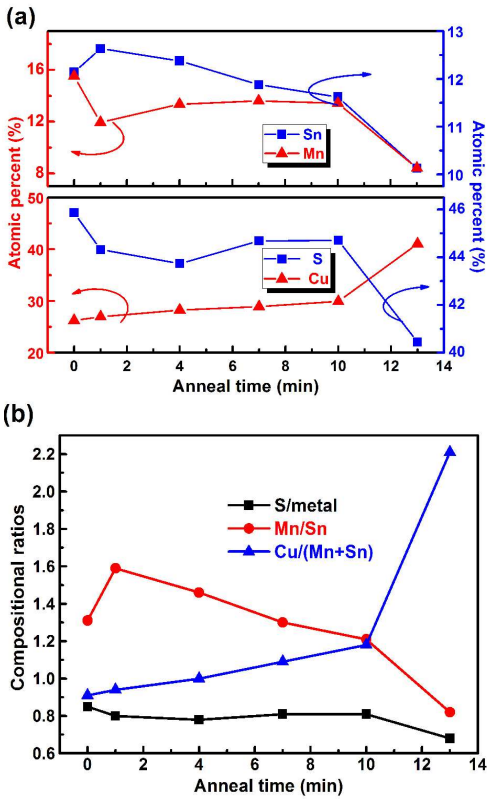

Fig. 5(a) chemical composition and **(b)** composition ratios of the precursor and sulfurized CMTS thin films.

3.4 Film morphology

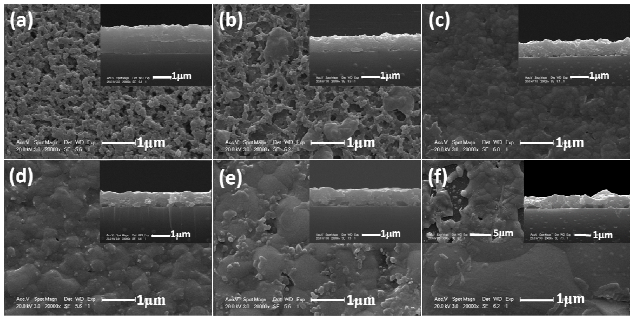

Fig. 6 Surface and cross-sectional SEM images of **(a)** CMTS-00, **(b)** CMTS-01, **(c)** CMTS-04, **(d)** CMTS-07, **(e)** CMTS-10, and **(f)** CMTS-13.

Fig. 6 shows the SEM images of the as-prepared precursor and of the films obtained at various annealing time. It can be seen that the as-prepared granular film has a crack structure with the particle size smaller than 100 nm. This is consistent with the broad XRD peaks. And resultant grain size is increased with increasing the annealing time. Upon post-anneal 1 min at 570 ºC, parts of the small nanoparticles generated and grew into large clusters of particles, as shown in Fig. 6b. The porosity (number of voids) of the film decreases sharply with increasing the annealing time to 4 min. Moreover, a relatively dense structure with large grains (~500 nm) and occasional voids developed when annealed time for 4 min. As the annealing time further increase to 10 min, the film exhibit more uniform and compact surface and a relatively enlarge in the grain size can be observed. The blurry and unsmooth surface could be caused by the bad cutting. As shown in Fig. 6f, the grain size increase to 2 μm as increase annealing time to 13 min, however, the film also exhibits large voids and pros structures (the inset of Fig. 6f gives an enlarge section image of CMTS-13 surface). The appearance of poor surface of CMTS-13 could be due to the overgrowth of the grains which has been confirmed by the XRD and Raman results.

The inset shows the cross-section SEM micrographs of those samples. As presented in the inset of Fig. 6a, the as-prepared precursor film shows the thickness around 1.9 μm and the other post-annealed thin films show the film thickness ~1.2 μm. As observed, the film thickness decreases dramatically upon the precursor films were post-annealed. We have reported previously that post-annealing the precursor film would lead the improvement of crystal quality and the decrease in thickness due to the decomposition and crystallization process.[4] Additionally, the film prepared at a longer annealing time (7, 10, and 13 min) have some grains extending from bottom to the top of the CMTS layer without large number of voids, relevant to the slight Sn loss during annealing process, which would lead to the voids at grain boundary and/or CMTS/SLG interface.[31] The film annealed for 13 min shows large grains that extend through the film and large voids at the CMTS/SLG interface. Even though the films consist of voids at the interface the overall adhesion of the film is good enough.

3.5 Optical properties

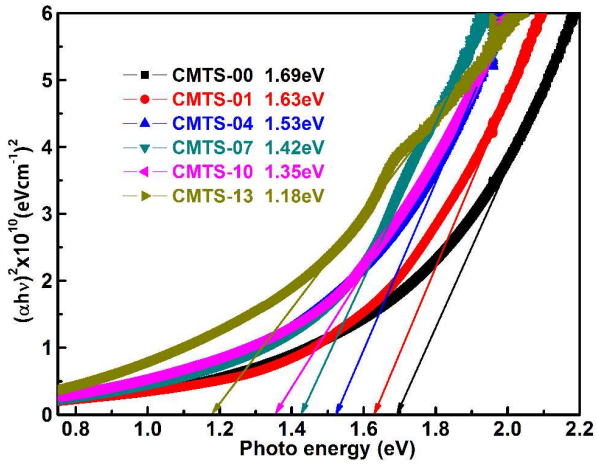

Fig. 7 Plot of $(\alpha h\nu)^2$ vs $h\nu$ for CMTS-00, CMTS-01, CMTS-04, CMTS-07, CMTS-10, and CMTS-13.

The optical transmittance spectrum of the CMTS thin films prepared with different anneal time was measured for the determination of band gap (E_g). According to the transmittance spectrum, the optical absorption coefficient α is calculated by the equation $\alpha = -\ln(T)/t$, where T is the transmittance of the film and t is the film thickness. The E_g of CMTS can be determined by applying equation $(\alpha h\nu)^2 = A(h\nu - E_g)$.[32] The optical band gap is determined by extrapolating the linear region of the plot $(\alpha h\nu)^2$ vs $h\nu$ and taking the intercept on the horizontal photon energy axis.

The typical $(\alpha h\nu)^2$ vs $h\nu$ plots of CMTS thin films are presented in Fig. 7. The determined band gap values of the as-prepared CMTS film and post-annealed films annealed at 1, 4, 7, 10, and 13 min are 1.69, 1.63, 1.53, 1.42, 1.35 and 1.18 eV, respectively. As presented, with increasing the anneal time, the band gap values shift to lower

energies gradually. The decrease of E_g values with increasing the annealing time can be attributed to the combined effect of crystalline quality improvement of CMTS thin films and the composition changes during the post-annealing process.[18, 27] On the one hand, the grain size increases and the grain boundary density decreases with the increase in anneal time, which would lead to the decreases of the scattering of electron at grain boundaries.[20] Therefore, electronic transition from valence band to conduction band becomes easily, and resulting in the decreasing of band gap values. Especially, the as-prepared thin film exhibits the smallest crystallite size (16.84 nm) and largest dislocation density (35.3×10^{14} lines/m^2) shows the largest band gap values (1.69 eV). On the other hand, Tanaka et al. investigated CZTS thin film as a function of the chemical composition of Cu/(Zn+Sn).[18] They found that the band gap energy of CZTS shifts to lower energies with the increase of Cu/(Zn+Sn) ratio. They attributed this to the changes in the degree of *p–d* hybridization between the Cu *d*-levels and S *p*-levels. In CZTS compound, the Valance Band Maximum (VBM) is due to antibonding of the S-*p* and Cu-*d* orbitals, whereas the Conduction Band Minimum (CBM) is S-*s* and Sn-*s* orbitals.[17, 18, 33] As discussed in the compositional analysis, the Cu content is slight enhanced with increasing the annealing time and the Cu/(Mn+Sn) ratio also increase from 0.91 to 2.21. Therefore, the band gap energy shifts of CMTS thin films might be also attributed to the increase of Cu content which results in the change of the degree of *p-d* hybridization between the Cu *d*-levels and S *p*-levels.

3.6 Device characterization

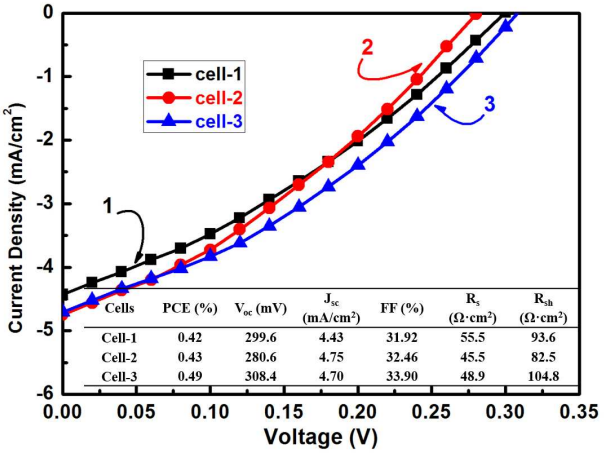

Cells	PCE (%)	V_{oc} (mV)	J_{sc} (mA/cm^2)	FF (%)	R_s (Ω·cm^2)	R_{sh} (Ω·cm^2)
Cell-1	0.42	299.6	4.43	31.92	55.5	93.6
Cell-2	0.43	280.6	4.75	32.46	45.5	82.5
Cell-3	0.49	308.4	4.70	33.90	48.9	104.8

Fig. 8 Current-voltage (J-V) characteristics of the solar cell devices fabricated with the CMTS-10 measured under AM1.5 simulated illumination.

The CMTS-10 absorber layer has been fabricated to photovoltaic device with the structure of AZO/i-ZnO/CdS/CMTS/Mo/glass configuration. Cell-1, 2 and 3 in Fig. 8 are made of CMTS-10 layer. J-V characteristics for the cell devices under simulated AM1.5 illumination are shown in Fig. 8, and all the device parameters are listed in the inset of Fig. 8. Cell-3 gives a better power conversion efficiency (PCEs) of 0.49% with a short-circuit current density (J_{sc}) of 4.70 mA/cm^2, an open-circuit potential (V_{oc}) of 308.4 mV, a fill factor (FF) of 33.9%, a high series resistance (R_s) of 48.9 Ω·cm^2, and a low shunt resistance (R_{sh}) of 104.8 Ω·cm^2. Note that this is the first report on the synthesis of CMTS solar cells. Cell-1 and 2 are other devices in the same sample which are close to the cell-3. They have PCEs of 0.42% and 0.43%, respectively, which indicates a relatively well controlled composition and quality distribution in the CMTS-10 absorber layer. In comparison the photovoltaic parameters of CMTS-10 device with those of higher CZTS device (PCE=6.6%, FF=57.2%, V_{oc}=581.4 mV, J_{sc}=19.9 mA/cm^2, R_s=5.3 Ω·cm^2 and R_{sh}=282.8 Ω·cm^2).[20] The PCEs in our device is predominantly limited by low V_{oc} (308.4 mV), low J_{sc} (4.70 mA/cm^2), and low FF (33.9%). The low R_{sh} can significantly leads to a low V_{oc}, and the high R_s may result in a low FF value as well as a low J_{sc}.[28] Generally, the high R_s might be attributed to the deterioration of transport charge transfer and the recombination of charge carriers at the CdS/CMTS interface, and the low R_{sh} can be ascribed to the small-grained CMTS layer.[20] Therefore, further optimization of the annealing conditions and interface treatment are important for fabricating a homogenous CMTS absorber layer composed of large grain size and pure phase in order to improve the device performance.

4. Conclusions

A simple and non-toxic spin-coating method is introduced to prepare CMTS thin films. The effect of annealing time on the film grow was optimized. Specifically, annealing for a short time (<10 min) lefts the synthesis incomplete, yielding films where secondary phases coexist with CMTS. The longer time annealing (10 min) yields film with upgraded degree of crystallinity, large grains and low dislocation density. Further increasing the anneal time to 13 min lead to the decomposition of CMTS into MnS, SnS and Cu_2S phases. The surface morphology shows that increasing the anneal time generally leads to improved film morphology and in the form of well-defined and densely packed CMTS grains. However, as further increased the annealing time to 13 min, the overgrowth of grains on the film is observed resulting a rough surface. The Cu content is generally increased with the increase of annealing time with the Cu/(Mn + Sn) ratio increased from 0.91 to 2.21. Analysis of transmission spectra for post-annealed CMTS thin films shows that the band gap energy shifts toward lower energies gradually with increasing the annealing time from 1.63 to 1.18 eV; especially, the as-prepared precursor film exhibits the largest band gap 1.69 eV. The decreasing of E_g values with increasing the anneal time can be attributed to the combined effect of the improvement of crystalline quality and Cu/(Mn + Sn) ratio in CMTS thin films. Most importantly, the CMTS solar cell (PEC=0.49%, J_{sc}=4.70 mA/cm^2, V_{oc}=308.4 mV, and FF=33.9%) with the commonly structure has been fabricated for the first time. This result offers the possibility for the application of CMTS absorber layer in low-cost solar cells by further optimization of the preparation process.

Acknowledgements

This work was supported by the National Natural Science Foundation of China (61474045), the State Key Basic Research Program of China (2013CB922300).

References

1 P. Jackson, D. Hariskos, R. Wuerz, O. Kiowski, A. Bauer, T. M. Friedlmeier, M. Powalla, Phys. Status Solidi RRL, 2015, 9, 28-31.
2 K. Ito and T. Nakazawa, Jpn. J. Appl. Phys., Part 1, 1988, 27, 2094-2097.
3 M. Quintero, E. Moreno, S. Alvarez, J. Marquina, C. Rincón, E. Qunitero, P. Grima, J.A. Heano, M.A. Macías, Rev. LatinAm. Metal. Mat., 2014, 34, 28-38.
4 L. Chen, H. Deng, J. Tao, W. Zhou, L. Sun, F. Yue, P. Yang, J. Chu, J. Alloys Compd., 2015, 640, 23-28.
5 X. Liang, P. Guo, G. Wang, R. Deng, D. Pan, X. Wei, RSC Adv., 2012, 2, 5044-5046.

6 C. Xu, H. Zhang, J. Parry, S. Perera, G. Long, H. Zeng, Sol. Energy Mater. Sol. Cells, 2013, 117, 357-362.
7 J.J. Scragg, T. Ericson, X. Fontané, V. Izquierdo-Roca, A. Pérez-Rod ríguez, T. Kubart, M. Edoffl, C. Platzer-Björkman, Prog. Photovolt: Res. Appl., 2014, 22, 10-17.
8 L. Yin, G. Cheng, Y. Feng, Z. Li, C. Yang, X. Xiao, RSC Adv., 2015, 5, 40369-40374.
9 S.C. Riha, B.A. Parkinson. A.L. Prieto, J. Am. Chem. Soc., 2009, 131, 12054-12055.
10 Y. Cui, R. Deng, G. Wang, D. Pan, J. Mater. Chem., 2012, 22, 23136-23139.
11 T. K. Todorov, J. Tang, S. Bag, O. Gunawan, T. Gokmen , Y. Zhu and D. B. Mitzi, Adv. Energy Mater., 2013, 3, 34-38.
12 W. Wang, M.T. Winkler, O. Gunawan, T. Gokmen, T.K. Todorov, Y. Zhu, D.B. Mitzi, Adv. Energy Mater., 2014, 4, 1301465.
13 Z. Su, K. Sun, Z. Han, Hong. Cui, F. Liu, Y. Lai, J. Li, X. Hao, Y. Liu, M.A. Green, J. Mater. Chem. A, 2014, 2, 500-509.
14 Y. Sun, Y. Zhang, H. Wang, M. Xie, Kai, Zong, H. Zheng, Y. Shu, J. Liu, H. Yan, M. Zhu, W. Lau, J. Mater. Chem. A, 2013, 1, 6880-6887.
15 K. Maeda, K. Tanaka, Y. Fukui, H. Uchiki, Sol. Energy Mater. Sol. Cells, 2011, 95, 2855-2860.
16 V. Tunuguntla, W. Chen, P. Shih, I. Shown, Y. Lin, J. Hwang, C. Lee, L. Chen, K. Chen, J. Mater. Chem. A, 2013, 00, 1-3.
17 J. Chen, Q. Chen, Y. Ni, Y. Yamaguchi, T. Wang, Z. Jia, X. Dou, S. Zhuang, J. Sol-Gel Sci. Technol., 2015, 75, 25-30.
18 K. Tanaka, Y. Fukui, N. Moritake, H. Uchiki, Sol. Energy Mater. Sol. Cells, 2011, 95, 838-842.
19 S. G. Kwon and T. Hyeon, Acc. Chem. Res., 2008, 41, 1696-1709.
20 J. Tao, K. Zhang, C. Zhang, L. Chen, H. Cao, J. Liu, J. Jiang, L. Sun, P. Yang, J. Chu, Chem. Commun., 2015, 51, 10337-10340.
21 S.Wang, Q. Y. Gao, J. C. Wang, J. Phys. Chem. B, 2005, 109, 17281-17289.
22 A. Begum, A. Hussain, A. Rahman, Beilstein J. Nanotechnol, 2012, 3, 438-443.
23 L. Chen, H. Deng, J. Cui, J. Tao, W. Zhou, H. Cao, L. Sun, P. Yang, J. Chu, J. Alloys Compd., 2015, 627, 388-392.
24 T. Fries, Y. Shapira, Phys. Rev. B, 1997, 56, 5424-5431.
25 M. Himmrich, H. Haeuseler, Spectrochim. Acta A, 1991, 47, 933-942.
26 A. Anastassiadou, E. Liarokapis, E. Anastassakis, Phys. Scripta., 1988, 38, 444-447.
27 J. He, L. Sun, Y. Chen, J. Jiang , P. Yang, J. Chu, RSC Adv., 2014, 4, 43080-43086.
28 J. Tao, J. Liu, J. He, K. Zhang, J. Jiang, L. Sun, P. Yang, J. Chu, RSC Adv., 2014, 4, 23977-23984.
29 D. Fan, R. Zhang, Y. Zhu, H. Peng, J. Zhang, J. Alloys Compd., 2014, 583, 566-573.
30 L. Sun, J. He, H. Kong, F. Yue, P. Yang, J. Chu, Sol. Energy Mater. Sol. Cells, 2011, 95, 2907-2913.
31 N. Moritake, Y. Fukui, M. Oonuki, K. Tanaka, H. Uchiki, Phys. Status Solidi C, 2009, 6, 1233-1236.
32 D. B. Khadka, J. Kim, J. Phys. Chem. C, 2014, 118, 14227-14237.
33 S. Chen, A. Walsh, Y. Luo, J. Yang, X.G. Gong, S.H. Wei, Phys. Rev. B, 2010, 82, 195203.